Performance of beam-type piezoelectric vibration energy harvester based on ZnO film fabrication and improved energy harvesting circuit

Shan Gao(高珊), Chong-Yang Zhang(张重扬), Hong-Rui Ao(敖宏瑞)†, and Hong-Yuan Jiang(姜洪源)

School of Mechatronics Engineering, Harbin Institute of Technology, Harbin 150001, *China*

(Received 12 February 2020; revised manuscript received 18 April 2020; accepted manuscript online 28 April 2020)

We demonstrate a piezoelectric vibration energy harvester with the ZnO piezoelectric film and an improved synchronous electric charge extraction energy harvesting circuit on the basis of the beam-type mechanical structure, especially investigate its output performance in vibration harvesting and ability to generate charges. By establishing the theoretical model for each of vibration and circuit, the numerical results of voltage and power output are obtained. By fabricating the prototype of this harvester, the quality of the sputtered film is explored. Theoretical and experimental analyses are conducted in open-circuit and closed-circuit conditions, where the open-circuit mode refers to the voltage output in relation to the ZnO film and external excitation, and the power output of the closed-circuit mode is relevant to resistance. Experimental findings show good agreement with the theoretical ones, in the output tendency. It is observed that the properties of ZnO film achieve regularly direct proportion to output performance under different excitations. Furthermore, a maximum experimental power output of 4.5 mW in a resistance range of 3 kΩ–8 kΩ is achieved by using an improved synchronous electric charge extraction circuit. The result is not only more than three times the power output of classic circuit, but also can broaden the resistance to a large range of 5 kΩ under an identical maximum value of power output. In this study we demonstrate the fundamental mechanism of piezoelectric materials under multiple conditions and take an example to show the methods of fabricating and testing the ZnO film. Furthermore, it may contribute to a novel energy harvesting circuit with high output performance.

Keywords: piezoelectric vibration energy harvester, beam-type structure, ZnO film, improved synchronous electric charge extraction circuit

PACS: 84.90.+a, 34.50.Ez, 77.84.–s, 29.27.–a **DOI:** 10.1088/1674-1056/ab8da1

1. Introduction

Piezoelectric vibration energy harvesting technology aims at collecting ambient mechanical energy and converting it into electricity efficiently. To improve the efficiency of the collection and conversion, three fundamental elements should be considered, *i.e.*, mechanical structures, piezoelectric materials, and energy harvesting circuits.[1]

In the mechanical structures,[2–5] spiral,[6,7] dandelion,[8] cymbal,[9] diaphragm type,[10] beam-type,[11,12] and L-shaped[13] structures, *etc.* have been developed in order to amplify the vibration amplitude from the environment and broaden the vibration frequency range of the harvester. Of them, cantilever beam-type structure is one of the simplest and most wildly used mechanical structures with relatively high output.[14,15] Therefore, many studies on beam-type structure have been conducted to test the properties of piezoelectric materials or measure the performance of the external energy harvesting circuit.

The piezoelectric materials[16,17] are another essential factor, which can be classified as three categories: piezoelectric crystal (such as quartz crystal, *etc.*); piezoelectric ceramics/piezoelectric polycrystalline crystal (*e.g.*, PZT, *etc.*) and new piezoelectric materials including piezoelectric polymers (*e.g.*, PVDF, *etc.*), piezoelectric semiconductor (*e.g.*, CdS, ZnO, AlN, *etc.*), and composite piezoelectric materials (*e.g.*, P(VDF-TrFE), *etc.*[18–20] Of them, PZT[21,22] is the most extensively used materials so far. However, ZnO[23,24] needs investigating because it is made more suitable for micro-nano scale and flexible devices, especially in piezoelectric film fabrication. The ZnO film can be produced by some methods, for example film-based extension, film magnetron sputtering, sol–gel, coating methods, *etc*. Generally, magnetron sputtering method is adopted due to its superiority in easy control and strong adhesion.[25,26]

The properties of piezoelectric materials are essential for evaluating the ability to generate charges.[27–29] In the same way, the collecting properties of follow-up energy harvesting circuit are also essential to measuring the capacity of charge conversion and electricity storage.[30–32] An excellent energy harvesting circuit not only can make the generated charges maximally converted into electricity, but also can continuously store and convert the electricity without any external power.[33–36] Up to now, most of energy harvesting circuits have been integrated into chips for commercial applications on a large-scale, such as standard harvesting circuit, Buck–Boost harvesting circuit, synchronous electric charge extraction har-

†Corresponding author. E-mail: hongrui_ao@hit.edu.cn

vesting circuit (SECE), *etc*.[37–41] However, these circuits cannot be effectively obtained, because disadvantages occur in the usage of energy harvesting circuits, including power loss and additional power requirement.

In this study, we develop an output test of piezoelectric energy harvester based on a cantilever beam-type structure. By adopting the ZnO piezoelectric material, power output in material properties is investigated and film preparation process and technical tests are also implemented. A thyristor-type switch is added to the SECE energy harvesting circuit to improve the efficiency of the power conversion and reduce the power loss. The thyristor switch conduces to accomplishing the periodical charge conversion and storage by its internal electrical characteristics. The circuit is on when a positive voltage is applied to the control gate, otherwise, it is off. Moreover, this internal positive feedback mechanism of the thyristor achieves continuously working by using the capacitance and diode, which conduces to the circuit self-powered operation.

The rest of the paper is organized as follows: In Section 2, the mechanical vibration and electrical circuit model of the beam-type harvester is established and the theoretical output voltage and power equations are derived. In Section 3, the ZnO film is fabricated by the magnetron sputtering method and then tested. The experimental setup is also introduced. In Section 4, open-circuit and closed-circuit outputs are compared theoretically and experimentally. The results are discussed and verified mutually. Finally, in Section 5 some conclusions are drawn from this study.

2. Theoretical analysis

The beam-type device is assembled by using the components as shown in Fig. 1, which consists of steel beam, mass block, Si substrate, and ZnO piezoelectric film with an Ag electrode attached to each of the top and bottom of the device. Specific dimensions of the beam-type structure are listed in Table 1. With a fixed and a free vibrating end, the external excitation is supposed to be applied to and felt on the free end. The mass block along with the free end of cantilever beam vibrates around the axis of the fixed end within permissible bending moment. The piezoelectric material ZnO generates charges under vibrating. When the device vibrates within a resonant frequency domain, the beam achieves maximum amplitude and maximally generates charges, which can be evaluated by voltage and power output theoretically.

Follow-up energy harvesting circuit is connected to the electrodes for charge conversion and electricity storage. The classic circuit of SECE[42,43] is shown in Fig. 2. It is one of the most wildly used and multiple loads suited circuits, whose synchronous switch periodically transfers the charges at the ends of capacitor to energy storage elements. However, extra electricity is consumed at the synchronous switch in addition to the unavoidable circuit loss. To solve the problem, in this article we present a new method of optimizing the power flow through extracting electric charges produced by a piezoelectric element and synchronized with the mechanical vibration, specifically an ISECE circuit with thyristor switch (shown in Fig. 3).

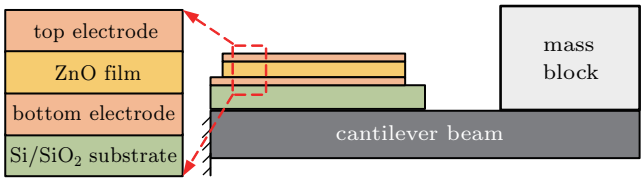

Fig. 1. Schematic diagram of piezoelectric energy harvesting vibrator.

Table 1. Dimensions of piezoelectric components in vibrator.

	Length/mm	Width/mm	Thickness/mm
Steel beam	80	12	2
Si substrate	10	10	0.625
ZnO film	8	8	0.30

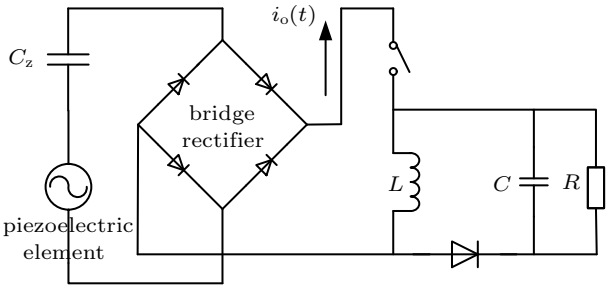

Fig. 2. Schematic diagram of SECE circuit.

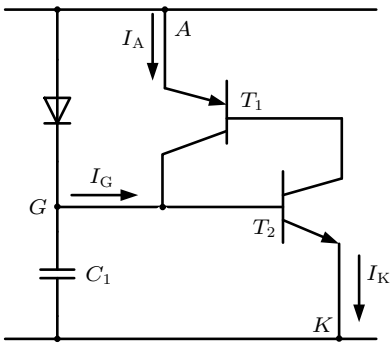

Fig. 3. Schematic diagram of thyristor switch.

With the internal electrical characteristics, the thyristor switch conduces to accomplishing the periodical charge conversion and storage. When a positive voltage is applied to the control gate, the thyristor is conducted, otherwise, the circuit is cut-off. Moreover, the internal positive feedback mechanism achieves continuously working by using the capacitance and diode. After that, the inductance completes the process of periodical conducting of the switch. The circuit diagram of ISECE is presented in Fig. 4. And the specifications of electronic components are listed in Table 2.

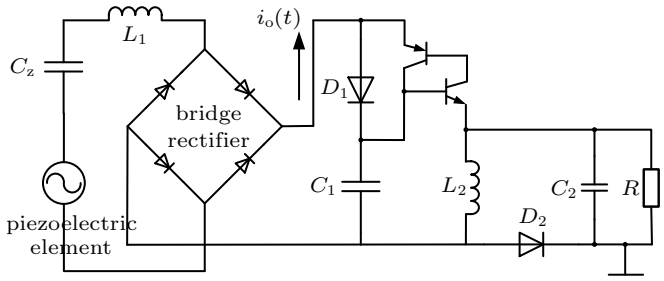

Fig. 4. Schematic diagram of ISECE circuit.

Table 2. Specifications of components in ISECE circuit.

Circuit component	Value
C_z	0.4 μF
C_1	5 μF
C_2	1 μF
L_1	2 H
L_2	0.8 H

The theoretical mathematic models of mechanical vibration and ISECE circuit are provided in the following subsections.

2.1. Mechanical vibration analysis

Direct piezoelectric effect is utilized because the ZnO film suffers compressive and tensile stress under the vibration of the cantilever beam. Therefore, the equations with piezoelectric coefficient d_{31} and d_{33} are expressed in the form of

$$\begin{cases} \sigma_1 = c_{31}^{\mathrm{E}}\delta_1 - d_{31}c_{31}^{\mathrm{E}}E_3, \\ D_3 = d_{31}c_{31}^{\mathrm{E}}\delta_1 + \varepsilon_{33}^{\mathrm{S}}E_3, \end{cases} \tag{1}$$

where σ_1 and δ_1 are the mechanical stress and strain, respectively; c_{31}^{E} and $\varepsilon_{33}^{\mathrm{S}}$ are the elastic compliance and clamped permittivity of the piezoelectric element, respectively; E_3 and D_3 are the electric field intensity and electric displacement, respectively.

In order to analyze the relationship between mechanical motion and output performance, the spring-damping-mass vibration model proposed by Williams and Yates[36,44] is adopted, and the obtained results are displayed in Fig. 5.

According to the D'Alembert's principle in mechanical dynamics, the equation of motion in the differential form for the system can be described as

$$m\ddot{x}_0(t) + c\dot{x}_0(t) + F(t) = -m\ddot{x}_i(t), \tag{2}$$

where m is the mass of the block, $x_i(t)$ is the sinusoidal displacement under which the cantilever beam vibrates, $x_0(t)$ is the displacement responsive to the vibration, c is the damping coefficient, and $F(t)$ is the equivalent internal force of the system, which can be defined as

$$F(t) = kx_0(t) + \alpha V(t), \tag{3}$$

with k and α being the stiffness and piezoelectric stress factor of the system, respectively, V being the output voltage, which is a function of time t, and αV being the piezoelectric coupling force. Thus, with Eq. (3), equation (2) can be rewritten as

$$m\ddot{x}_0(t) + c\dot{x}_0(t) + kx_0(t) + \alpha V(t) = -m\ddot{x}_i(t). \tag{4}$$

The electric field intensity E_3 and the mechanical strain δ_1 in Eq. (1) are expressed as

$$E_3 = -\frac{V(t)}{h_z}, \tag{5a}$$

$$\delta_1 = \frac{x_0(t)}{h_z}, \tag{5b}$$

where h is the thickness of the layer of piezoelectric component and the subscript z represents ZnO film. Substituting Eqs. (5a) and (5b) into Eq. (1), the piezoelectric equation can be rewritten in terms of mechanical and electrical mode parameters

$$kx_0(t) + \alpha V = c_{31}^{\mathrm{E}}\frac{x_0(t)}{t_z}A + d_{31}c_{31}^{\mathrm{E}}\frac{V(t)}{t_z}A, \tag{6}$$

where A is the effective area of the piezoelectric layer. It is obvious to draw a conclusion with one-to-one correspondence as follows:

$$\begin{cases} k = c_{31}^{\mathrm{E}}\dfrac{A}{t_z}, \\ \alpha = c_{31}^{\mathrm{E}}d_{31}\dfrac{A}{t_z}. \end{cases} \tag{7}$$

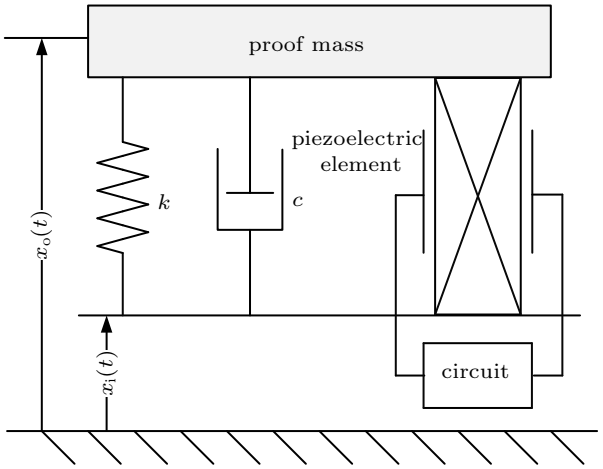

Fig. 5. Schematic diagram of spring–damping–mass vibration model.

According to Gauss theorem of electrostatic field with dielectric, the quantities of electric charge Q can be obtained below:

$$\begin{cases} \oiint_S D\mathrm{d}s = Q, \\ D_3 = \dfrac{Q}{A}. \end{cases} \tag{8}$$

Substitute Eq. (8) into Eq. (1), the equation of Q is rewritten as

$$Q = d_{31}\frac{A}{t_z}x_0(t) - \varepsilon_{33}^{S}\frac{A}{t_z}V(t). \tag{9}$$

Since the current intensity $i(t)$ satisfies the charge equation in differential form, *i.e.*, $i(t) = \mathrm{d}Q/\mathrm{d}t$. It can be expressed at

$$i(t) = d_{31}c_{31}^{E}\frac{A}{t_z}\dot{x}_0(t) - \varepsilon_{33}^{S}\frac{A}{t_z}\dot{V}(t). \tag{10}$$

In a spring–damping–mass vibrating system, $i(t)$ is defended as $i(t) = V(t)/R$, where R is the resistance including external load resistance R_l and piezoelectric resistance R_p. Because these two resistances are in parallel connection, and $R \gg R_p$. Hence, R can be estimated at R_l and Eq. (10) can be rewritten as

$$C_p\dot{V}(t) + \frac{V(t)}{R} - \alpha\dot{x}_0(t) = 0, \tag{11}$$

where $C_p = \varepsilon_{33}^{S}A/t_z$, and $\alpha = d_{31}c_{31}^{E}A/t_z$.

Applying Laplace transformation to Eqs. (4) and (11) with zero initial condition, the resulting equations are expressed as

$$\begin{cases} X_0\left(s^2 + \dfrac{c}{m}s + \dfrac{k}{m}\right) = -X_i s^2 - \dfrac{\alpha}{m}V, \\ \alpha s X_0 = C_p V s + \dfrac{V}{R}, \end{cases} \tag{12}$$

where s and X are the Laplacian variables corresponding to t and $x(t)$, respectively, ω_n and ζ are the resonant frequency and damping ratio in the vibration system, expressed, respectively, as

$$\begin{cases} \omega_n = \sqrt{\dfrac{k}{m}}, \\ \zeta = \dfrac{c}{2\sqrt{km}}. \end{cases} \tag{13}$$

In accordance with the equations above and by replacing s into $\mathrm{j}\omega$, the relationship between output voltage and deformation response can be expressed as

$$\left|\frac{V}{X_0}\right| = \frac{\omega\dfrac{\alpha}{C_p}}{\sqrt{\left\{\left[\dfrac{\omega_n^2}{RC_p} - \left(\dfrac{1}{RC_p} + 2\zeta\omega_n\right)\omega^2\right]^2 + \omega^2\left[\omega_n^2 + \dfrac{\alpha^2}{kC_p}\omega_n^2 + \dfrac{2\zeta\omega_n}{RC_p} - \omega^2\right]^2\right\}}}. \tag{14}$$

As is well known, the best output performance occurs at the resonant frequency of the harvester, that is, $\omega = \omega_n$. Therefore, the maximum voltage output satisfies the following equation:

$$\left|\frac{V}{X_0}\right| = \frac{\dfrac{\alpha}{C_p}}{\omega_n\sqrt{(2\zeta\omega_n)^2 + \left(\dfrac{\alpha^2\omega_n}{kC_p} + \dfrac{2\zeta}{RC_p}\right)^2}}. \tag{15}$$

It can be seen that the voltage output is mainly related to the resonant frequency, damping ratio, and performance parameters of ZnO film.

2.2. ISECE circuit analysis

The working stages of ISECE circuit for measuring voltage are as follows:

(i) In the first stage, generated charges conduct to the surface of electrodes and continuously flow into the capacitor. At the same time, the bridge rectifier is reversely biased with no output voltage. This situation lasts until the voltage across both ends of the capacitor is equal to the output voltage V_c.

(ii) In the second stage, the current flows into filter capacitor and load. In this stage, the output voltage is fixed at V_c and $-V_c$.

(iii) The interval time u between first and second stage is the duration from V_c to $-V_c$, determined by[45]

$$\cos(u) = 1 - \frac{2V_c\omega C_z}{I_z}. \tag{16}$$

An assumption is made that the diode is a conductor and the load is treated as an open circuit. Based on the parallel relationship between the filter and internal capacitor, the electrical characteristics of the cantilever beam structure can be expressed as a sinusoidal output current, $i_o(t)$. It depends on the mechanical excitation level of the piezoelectric material, which is the open-circuit output voltage V_c. Therefore, the output current can be modeled as

$$i_o(t) = \begin{cases} 0, & 0 \leqslant t < u/\omega, \\ \dfrac{C}{C_z + C}I_z\left|\sin(\omega t)\right|, & u/\omega \leqslant t < \pi/\omega, \end{cases} \tag{17}$$

where the output current is assumed to be given from the capacitance C_z connected in parallel with the electrode. The current consumed on piezoelectric material can be ignored when the filter capacitance is much larger than the internal capacitance. An AC–DC rectifier is connected to the output of the piezoelectric device. Therefore, the DC component of the output current can be expressed as

$$\langle i_o(t)\rangle = \frac{2I_z}{\pi} - \frac{2V_c\omega C_z}{\pi}, \tag{18}$$

and the output power of the piezoelectric element is the product of the output current and the rectifier capacitor voltage, which can be expressed as

$$\langle P(t)\rangle = \frac{2V_c}{\pi}\left(I_z - V_c\omega C_z\right). \tag{19}$$

In conclusion, the maximum voltage power output combined with Eq. (14) can be expressed as

$$V_c = \frac{R\alpha}{RC_z\omega + (\pi/2)}\omega x_0, \tag{20}$$

and the maximum power output is

$$P_{\max} = \frac{V_c^2}{R} = \frac{R\alpha^2}{\left(RC_z\omega + (\pi/2)\right)^2}\omega^2 x_0^2. \tag{21}$$

3. Device fabrication and experimental setup

3.1. Device fabrication

Beam-type piezoelectric energy harvester with ZnO film is fabricated in parts, including beam, substrate, electrodes and ZnO film. First, the general incision method is used to cut steel and Si into appropriate dimensions. Then, the flanged paste method is employed to ensure that the top and bottom Ag electrodes are stuck firmly to the ZnO film, which confirms the flatness of electrodes after connecting to wires. Next, the magnetron sputtering method is utilized to prepare the ZnO film, which is the most complicating part in this fabrication. The sputtering chamber is set in an approximate vacuum environment, and the target material ZnO is completely sputtered on the Si substrate. The conditions of the sputtering method are given in Table 3. The ZnO film thickness of the device is 5 μm.

Table 3. Deposition parameters of ZnO film.

Deposition parameters	Values
Target	ZnO (99.99%)
Substrate	silica slice (110)
Target-substrate distance	50 mm
Deposition time	6.5 h
Pressure Ar:O_2	1.0 Pa 4:1
Substrate temperature	200 °C
Sputtering power	110 W

3.2. Fabrication tests

The properties of the film manufacturing technique are tested in two aspects. In the first aspect, roughness, grain diameter and surface topography are evaluated by an atomic force microscope (AFM) (Dimension Fastscan). With relatively low measured values, small and little particles are detected on the surface, which means that the film is smooth and homogeneous. In the second aspect, the piezoelectric properties of ZnO come from c-axis-preferred orientation of crystal lattice. Materials with good piezoelectric properties should grow intensively along the vertical c axis in microstructure. Therefore, XRD spectral line detected by x-ray diffractometer (Panalytical Empyrean) can validate the quality of ZnO preparation. And the XRD spectrum should display one strong Bragg diffraction peak.

In this work, figures 6 and 7 show the surface topography and XRD spectrum of the sputtered ZnO film, and the specific testing values are presented in Table 4. It can be seen that the values of roughness and grain diameter in this study are on a nanoscale and lower than those on generally machined surface at a micro level. An obviously strongest peak appears in the ⟨002⟩ axis, meaning that the c-axis of this ZnO film is successfully achieved. Therefore, the fabricated ZnO film achieves good surface quality and piezoelectric properties.

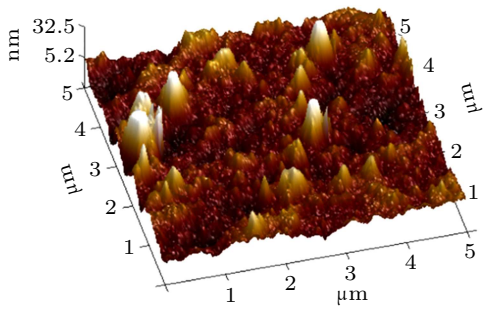

Fig. 6. Surface topography of sputtered ZnO film under magnification factor of 8000.

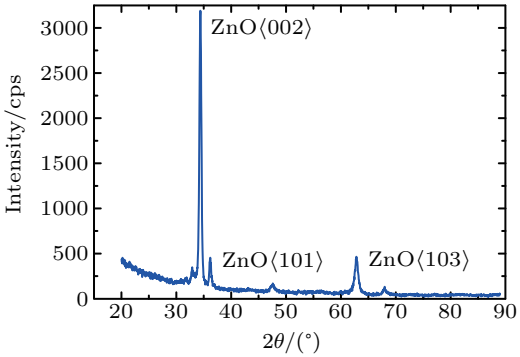

Fig. 7. XRD spectrum of sputtered ZnO film.

Table 4. Surface topography testing values of ZnO film.

Parameter	Value
Overall roughness/nm	1.46
Local maximum roughness/nm	1.96
Relatively intensity	48
Grain diameter/nm	17.4
Diffraction angle $2\theta/(^\circ)$	34.44
Standard deviation	0.01
Full width at half maximum/(°)	0.45

3.3. Experimental setup

Figure 8 describes the flowchart of the experimental setup. It can be explained below. The beam-type piezoelectric vibration energy harvester is vertically driven by the exciter, which is controlled by the power amplifier then connected to an oscilloscope. A sinusoidal signal coming from

the signal generator is applied by an exciter to the energy harvester directly. The output of harvester is monitored by the accelerometer and managed by the ISCE energy harvesting circuit. Through the data acquisition module in computer, the experimental results are collected by the oscilloscope and charge amplifier. The actual diagram of the experimental system is shown in Fig. 9.

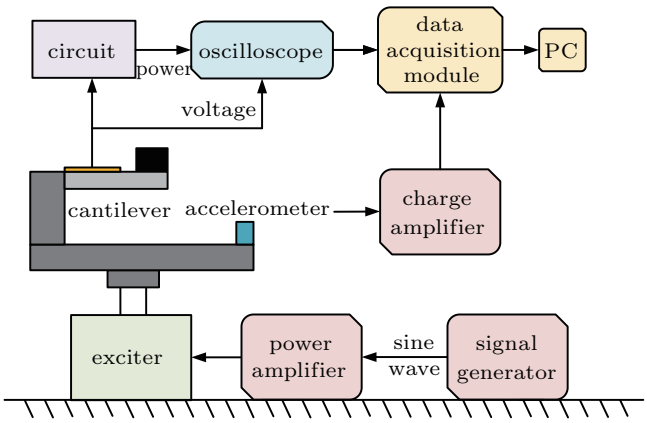

Fig. 8. Schematic diagram of experimental setup.

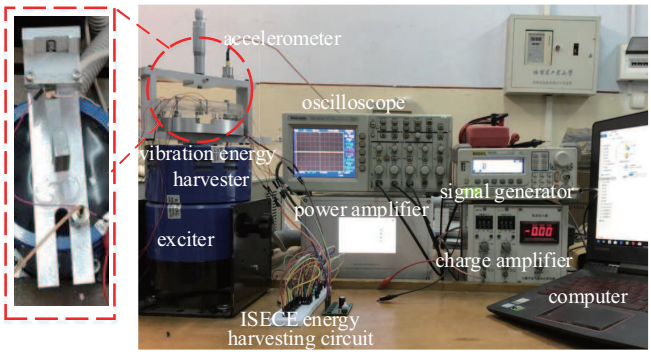

Fig. 9. Experimental apparatus of whole energy harvester testing system.

The specific functions of these devices are described below.

(I) Signal generator is adjusted to produce a sinusoidal signal and transfer it to the following power amplifier. Power amplifier as a processing unit amplifies the signal to an extent that reaches the demand of the exciter. Suitable sine wave is delivered to the vibration exciter.

(II) Vibration exciter drives the harvester vibrating together under sinusoidal wave. An accelerometer is attached to the basement in order to monitor the condition of the vibration and transfer the feedback information to the charge amplifier. The charge amplifier plays a role in amplifying the charges and feeding the signal output to PC.

(III) Direct signals output from the harvester are shown in oscilloscope including the output voltage, frequency, phase, *etc*. After linking with the resistance, calculated power output from the harvester is acquired by the data acquisition module for further processing.

4. Results and discussion

4.1. Theoretical results

Based on the equations in Section 2, the theoretical voltage and power output are derived by using software MATLAB, COMSOL, and Multisim. The mechanical model is used to discuss the dependence of the thickness of ZnO film and external force on frequency. And the ISECE model is used to explore the dependence of output performance on time and resistance. The results are shown in the following parts.

4.1.1. Mechanical vibration (open-circuit) results

Without adding follow-up circuit, the harvester can be seen as an open-circuit mode, whose output is in the form of voltage. In Eq. (15), the relationship between voltage output and ZnO parameters (such as damping ratio and deformation output) is demonstrated. Considering the actual environment, the damping ratio of ZnO is affected by the thickness and surface quality of the ZnO film; the deformation output is affected by the external excitation. Therefore, in order to facilitate the experiment, in this part, we provide the results of voltage output *versus* vibrational frequency under different thickness of ZnO film and external forces. The obtained results are presented in Figs. 10 and 11, respectively.

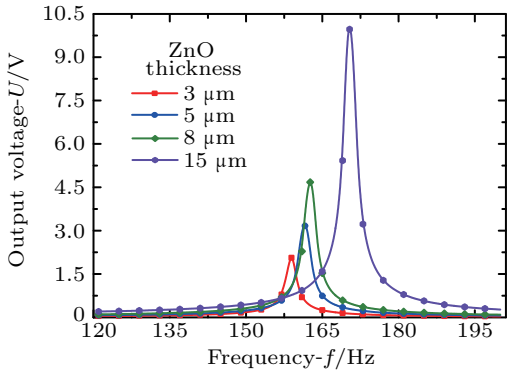

Fig. 10. Plots of theoretical voltage output U *versus* frequency f for four different thickness values of ZnO film.

Figure 10 shows the plots under a sinusoidal force of 2 N with different thicknesses of ZnO film. It can be seen that the voltage output curves have their own resonant frequencies and peak voltages. When the thickness increases from 3 μm to 15 μm (maximum allowable thickness of magnetron sputtering instrument), on the one hand, the resonant frequency is slightly shifted rightwards by approximately 10 Hz. The rightward shift of the resonant frequency is due to the increase of the harvester in thickness. Once the film turns thicker, the rigidity of vibrator increases, which leads the vibration frequency to slightly increase. Although the consequence of addition in thickness is obvious, the slight fluctuation in resonant frequency can be neglected compared with that in the wide-ranged frequency in the environment. On the other hand, the maximum voltages of different films range from 2 V (for

5-μm-thick film) to 10 V (for 15-μm-thick film). Comparing these values, the proportional relations between maximum voltage output and corresponding thickness are found to be almost the same. Hence, thick film of piezoelectric material should be employed to enhance voltage output, but processing and frequency required conditions should be considered.

Figure 11 shows the plots of output voltage *versus* frequency of a 5-μm-thick ZnO film under different amplitudes of sinusoidal forces. When the external force increases from 1 N to 4 N, the maximum voltages are at an identical resonant frequency of 161.5 Hz, which indicates that the resonant frequency is unrelated to the external force. It is because the resonant frequency (defined by Eq. (13)) is an inherent quality and related to rigidity of the device. Therefore, it can be found that the external force, acceleration or other excitations have little influence on it. When the maximum voltage output increases from 1.4 V to 5.5 V, the maximum voltages are almost in direct proportion to external force. Besides, the greater the external forces are, the larger the maximum voltage output can be obtained. Hence, a large external force should be added to the harvester to gain higher output, but the force should be within the allowable stress, otherwise, the harvester will be broken down.

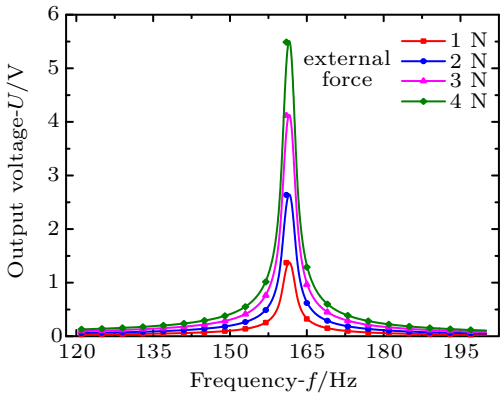

Fig. 11. Plots of theoretical voltage output U *versus* frequency f of ZnO film under four different external forces.

According to Figs. 10 and 11, it can be inferred that the curves of the voltage output *versus* frequency in different conditions have the same shape. With f increasing from 120 Hz to 200 Hz, each voltage output increases dramatically from 0 to the maximum value, which is corresponding to its resonant frequency. Then the output slumps to almost 0 at the same speed as that of the increase. Taking a certain voltage as the effective voltage, for example 0.5 V, the frequency domain where the voltage exceeds 0.5 V is regarded as the effective frequency domain. In Fig. 9, the maximum effective frequency domain is 9 Hz, which is the result of 15-μm-thick ZnO film compared with those of ZnO films with other thickness values. Similarly, in Fig. 10, the maximum frequency domain is 17 Hz of 4-N external force. Obviously, the frequency domain is a significant method to evaluate output performance. The wider domain it possesses, the more voltage can be accumulated.

4.1.2. Circuit (closed-circuit) results

With adding a follow-up circuit, the harvester can be seen as a closed-circuit mode, whose output is in the form of power. In order to test the ability of ISECE circuit to generate the charges, the theoretical closed-circuit output is simulated by comparing the SECE circuit. In Subsection 2.2, equations display the output power focusing on external resistance according to Eqs. (20) and (21). Figure 12 shows the numerical relation between power output and resistance.

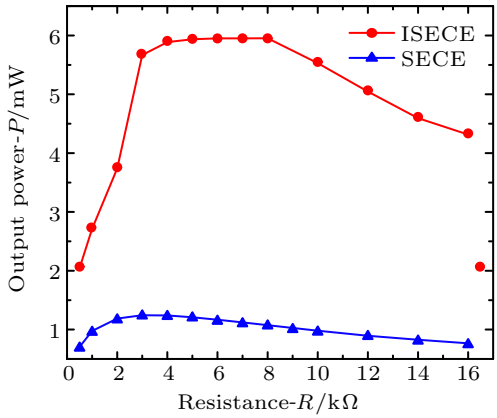

Fig. 12. Plots of theoretical output power P *versus* resistance in SECE and ISECE circuits.

Taking the power output within 16 kΩ for example, the curves in Fig. 12 clearly demonstrate the variations of power output with resistance for the ISECE and SECE circuits. On the one side, the curves obviously demonstrate the huge gap between the output of ISECE circuit and the output of SECE circuits. The power of ISECE circuit displays high output level, which rises rapidly from 2 mW to the climax of 6 mW, then falls gradually to 4.3 mW. However, the power output of SECE circuit shows stabilized trend with maximum power of 1.3 mW, which is lower than that of the ISECE. In the ISECE circuit, the slight distinction in power result indicates the stability in output performance. Moreover, the high level of power output can improve storage efficiency and reduce charge losses in the harvester. On the other hand, the high-power output of ISECE circuit is maintained at 6 mW in a range from 3 kΩ to 8 kΩ. It is suggested that the output performance can be maintained at a stable output level when the resistance is any value between 3 kΩ and 8 kΩ. This outstanding advantage makes the experimental operation flexible and reflects good applicability. Although the SECE circuit has better applicability due to its stable curve trend, the low power will reduce the output. Hence, the ISECE circuit is expected to have an energy harvesting circuit with high output, flexible choice of resistance, low charge loss and good applicability.

4.2. Experimental results

Using the setup in Section 3, the experiments are undertaken in order to verify the theoretical simulation results. Firstly, the dependence of open-circuit voltage on frequency is investigated. Typically, external excitations like force and acceleration act on the harvester through the same mechanism. Thus, acceleration is selected in this research because it is easier to control through signal generator than through force. Secondly, closed-circuit output is conducted under the same conditions as those in theoretical simulations. The results are in the following parts.

4.2.1. Mechanical vibration (open-circuit) results

In the experiments, accelerations of 0.5 g–1.5 g are applied to the harvester, which can be converted into external force of 1 N–3 N by calculating with the equivalent mass of the whole device. And the corresponding voltages are presented in Fig. 13. In accordance with the curves, first of all, although other resonant frequencies of the device can be tested, they are unable to adapt to the actual environment. Hence, two resonant frequencies are derived, which are 170 Hz and 279 Hz, respectively in the low frequency range. Next, the curves clearly demonstrate that the tendencies are not affected when the harvester is subjected to different forces. Not only the resonant frequencies remain unchanged, but also the positions of peak and trough display identically. Then, when the force is adjusted from 1 N to 3 N, the maximum voltages under first resonant frequency are 1.2 V, 2.4 V, and 3.6 V, respectively; and 1 V, 2 V, and 3 V, respectively under second resonant frequency. On the basis of these values it can be inferred that the output concerning with the resonant frequency is significantly regular, *i.e.*, obviously in direct proportion. Hence, the conclusion accords with the theoretical result shown in Fig. 13. In addition, the device can harvest more energy under resonant frequency with a large external force.

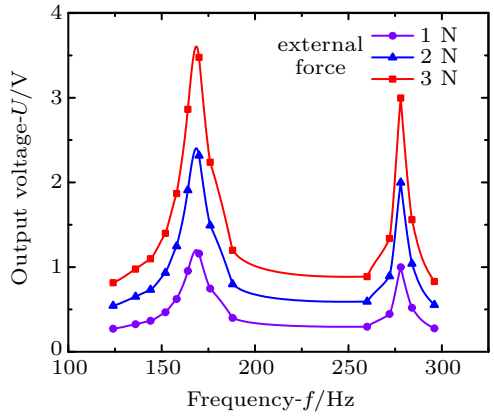

Fig. 13. Plots of experimental voltage output U *versus* frequency f under three different forces.

4.2.2. Circuit (closed-circuit) results

Experiments on harvesting circuits are undertaken to justify the theoretical results, so it totally duplicates the theoretical results of ISECE and SECE circuits. The corresponding powers are shown in Fig. 14. The same variation trends but with a little difference in value are displayed in comparison with the curves in Fig. 12. As the power losses in wires and electrical components cannot be neglected in practice, a slightly drop of power in the experiment is inevitable. As can be seen, the power output of ISECE circuit has a decline of 1.5 mW in maximum level and 1 mW in average level. Similarly, the power output of SECE circuit has a decrease of 0.15 mW in maximum level and 0.175 mW in average level. Although the decline in power output of ISECE circuit is much higher, there is no doubt that the ISECE circuit is superior to the SECE for its better output performance.

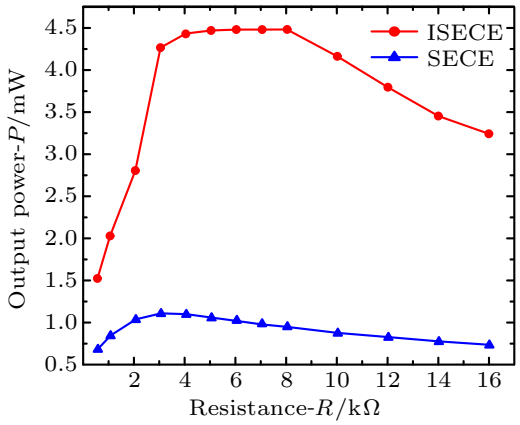

Fig. 14. Experimental output power P *versus* resistance R in SECE and ISECE circuits.

In this study, we investigate the output performance of a piezoelectric vibration energy harvester with ZnO piezoelectric film and improve synchronous electric charge extraction energy harvesting circuit in vibration harvesting and ability to generate charges on the basis of the beam-type mechanical structure. The results are illustrated theoretically and experimentally as presented above. They have been validated to support and add to the findings of Abdelmoula and Dai,[46] in which the output performance of the cantilevered beam structure under sinusoidal harmonic excitation is displayed. The results in the paper make sense as a reference with the same condition. In consequence, the equations of output voltage and curves of output power show the same tendencies as those in this work, whose accuracy of the conclusion is proved. In addition, this work also demonstrates further output voltage and power accurately in value, which help to complete the work of Abdelmoula and Dai.[46] In the long term, this study has paved the way for improving the defection of existing energy harvesting circuits and investigating their output performances. Also, tests and fabrications of ZnO film and beam-type structure offer an example of experiments on piezoelectric harvesters. However, the cantilever beam-type structure cannot totally represent harvesters and the tests are conducted within small ranges. For example, The experiments on a large

scale of frequency and resistance may not performed in the same way (Yildirim & Ghayesh, 2016).[47] Therefore, the further step in this study should be replicated with other materials and a large scale of testing data to complete and verify the research findings.

5. Conclusions

The purpose of the test is to investigate the ability of ZnO film to generate and convert charges and improve synchronous electric charge extraction circuit on the basis of the beam-type piezoelectric vibration energy harvester. The numerical results of voltage and power output are obtained through establishing the theoretical models. The theoretical analyses are simulated and the experimental tests are conducted in order to validate the accuracy of model results. In this test, a maximum open-circuit voltage is achieved at 3.6 V under 3-N force and 5-μm-thick ZnO film at a resonant frequency of 170 Hz. With 4.5-mW maximum output in a resistance range of 3 kΩ–8 kΩ, the harvester with the ISECE circuit can produce up to three times more than the power output of SECE circuit. It is indicted that the voltage of open-circuit mode increases in direct proportion to the thickness of the ZnO film and external excitation. The closed-circuit power output of the ISECE circuit is also significantly higher than that of the SECE. And the ISECE circuit can effectively enhance the sustainable capacity of maximum output. Overall, in this study we improve the synchronous electric charge extraction energy harvesting circuit and verify its excellent self-powered and low-loss properties, which will be applied to multiple energy harvesting systems. Also, in this research, we introduce the sputtered ZnO film into the beam-type harvester with the ISECE circuit, demonstrated by multiple testing methods, which can be used as an experimental technique for preparing piezoelectric materials or structures or circuits. Accordingly, the future work will focus on completing the large-scale experimental conditions by integrating multiple piezoelectric materials with novel structures.

References

[1] Wang P, Du H and Shen S 2012 *Appl. Surf. Sci.* **258** 9510
[2] Li X, Upadrashta D, Yu K and Yang Y 2018 *Energ. Convers. Manag.* **176** 69
[3] Fan K Q, Xu C H, Wang W D and Fang Y 2014 *Chin. Phys. B* **23** 084501
[4] Erturk A and Inman D J 2008 *Smart Mater. Struct.* **17** 065016
[5] Yang Z, Wang Y Q, Zuo L and Zu J 2017 *Energ. Convers. Manag.* **148** 260
[6] Fan K Q, Ming Z F, Xu C H and Chao F B 2013 *Chin. Phys. B* **22** 104502
[7] Zhang L, Lu J, Takei R, Makimoto N, Itoh T and Kobayashi T 2016 *Rev. Sci. Instrum.* **87** 085005
[8] Chen R, Ren L, Xia H, Yuan X and Liu X 2015 *Sens. Actuat. A-Phys.* **230** 1
[9] Kim H W, Batra A, Priya S, Uchino K, Markley D, Newnham R E and Hofmann H F 2004 *Jpn. J. Appl. Phys.* **43** 6178
[10] Kuehne I, Marinkovic D, Eckstein G and Seidel H 2008 *Sens. Actuat. A-Phys.* **142** 292
[11] Bai Y, Tofel P, Hadas Z, Smilek J, Losak P, Skarvada P and Macku R 2018 *Mech. Syst. Signal Pr.* **106** 303
[12] Erturk A and Inman D J 2008 *J. Intel. Mat. Syst. Str.* **19** 1311
[13] Erturk A, Sodano H A, Renno J M and Inman D J 2009 *J. Intel. Mat. Syst. Str.* **20** 529
[14] Zhao S and Erturk A 2013 *Smart Mater. Struct.* **22** 015002
[15] Izadgoshasb I, Lim Y Y, Lake N, Tang L, Padilla R V and Kashiwao T 2018 *Energ. Convers. Manag.* **161** 66
[16] Lee C S, Joo J, Han S and Koh S K 2004 *Appl. Phys. Lett.* **85** 1841
[17] Li H, Tian C and Deng Z D 2014 *Appl. Phys. Rev.* **1** 041301
[18] Bhavanasi V, Kumar V, Parida K, Wang J and Lee P S 2016 *Acs Appl. Mater. Inter.* **8** 521
[19] Kanno I, Ichida T, Adachi K, Kotera H, Shibata K and Mishima T 2012 *Sens. Actuat. A-Phys.* **179** 132
[20] Wang Y, Zhang X, Guo X, Li D, Cui B, Wu K, Yun J, Mao J, Xi L and Zuo Y 2018 *J. Mater. Sci.* **53** 13081
[21] Shen D, Park J H, Ajitsaria J, Choe S Y, Wikle H C and Kim D J 2008 *J. Micromech. Microeng.* **18** 055017
[22] Platt S R, Farritor S and Haider H 2005 *IEEE-ASME T. Mech.* **10** 240
[23] Zhang Z, Kang Z, Liao Q L, Zhang X M and Zhang Y 2017 *Chin. Phys. B* **26** 118102
[24] Yuan Y, Du H, Wang P, Chow K S, Zhang M, Yu S and Liu B 2013 *Sens. Actuat. A-Phys.* **194** 75
[25] Wang P, Du H, Shen S, *et al.* 2012 *Nanoscale Res. Lett.* **7** 176
[26] Li B S, Xiao Z Y, Ma J G and Liu Y C 2017 *Chin. Phys. B* **26** 117101
[27] Li J and Wang X 2017 *APL Mater.* **5** 073801
[28] Yang Z and Zu J 2016 *Energ. Convers. Manag.* **122** 321
[29] Wu J, Shi H, Zhao T, Yu Y and Dong S 2016 *Adv. Funct. Mater.* **26** 7186
[30] Kumar C N 2015 *J. Phys.: Conf. Ser.* **662** 012031
[31] Kwon S C, Onoda J and Oh H U 2019 *Mech. Syst. Signal Pr.* **117** 361
[32] Pan J M, Qin W Y, Deng W Z and Zhou H L 2019 *Chin. Phys. B* **28** 017701
[33] Wang X, Shi Z, Wang J and Xiang H 2016 *Smart Mater. Struct.* **25** 055005
[34] Yang Z, Zhu Y and Zu J 2015 *Smart Mater. Struct.* **24** 025028
[35] Akaydin H D, Elvin N and Andreopoulos Y 2012 *Smart Mater. Struct.* **21** 025007
[36] Lefeuvre E, Badel A, Richard C, Petit L and Guyomar D 2006 *Sens. Actuat. A-Phys.* **126** 405
[37] Wu Y, Badel A, Formosa F, Liu W and Agbossou 2014 *J. Intel. Mat. Syst. Str.* **25** 2165
[38] Liang J, Zhao Y and Zhao K 2019 *IEEE T. Power Electr.* **34** 275
[39] Roundy S and Tola J 2014 *Smart Mater. Struct.* **23** 105004
[40] Khan A, Abas Z, Soo Kim H and Oh I K 2016 *Smart Mater. Struct.* **25** 053002
[41] Xia H, Xia Y, Ye Y, Qian L, Shi G and Chen R 2018 *IEEE Sens. J.* **18** 6235
[42] Arroyo E and Badel A 2011 *Sens. Actuat. A-Phys.* **171** 266
[43] Lefeuvre E, Badel A, Richard C and Guyomar D 2005 *J. Intel. Mat. Syst. Str.* **16** 865
[44] Williams C B and Yates R B 1996 *Sens. Actuat. A-Phys.* **52** 8
[45] Geffrey K O, Heath F H and George A L 2003 *IEEE T. Power Electr.* **8** 696
[46] Abdelmoula H, Dai H L, Abdelkefi A and Wang L 2017 *Smart Mater. Struct.* **26** 095013
[47] Yildirim T, Ghayesh M H, Searle T, Li W and Alici G 2017 *J. Energ. Resour.-ASME* **139** 032001